

pubs.acs.org/JPCL Letter

Nanoscale Surface-Induced Unfolding of Single Fibronectin Is Restricted by Serum Albumin Crowding

Lauren A. Warning, Qingfeng Zhang, Rashad Baiyasi, Christy F. Landes,* and Stephan Link*



Cite This: J. Phys. Chem. Lett. 2020, 11, 1170-1177



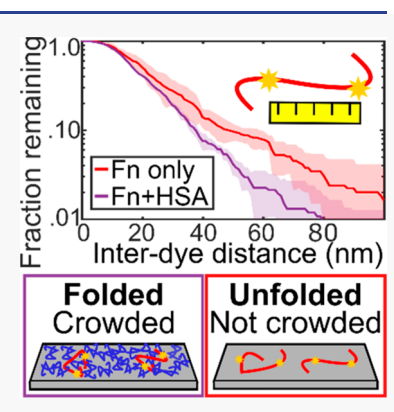
ACCESS

Metrics & More

Article Recommendations

Supporting Information

ABSTRACT: Understanding nanoscale protein conformational changes at solid—liquid interfaces is critical for predicting how proteins will impact the performance of biomaterials in vivo. Crowding is an important contributor to conformational stability. Here we apply single-molecule high resolution imaging with photobleaching to directly measure dye-conjugated fibronectin's unfolding in varying conditions of crowding with human serum albumin on aminosilanized glass. Using this approach, we identify serum albumin's crowding mechanism. We find that fibronectin achieves larger degrees of unfolding when not crowded by coadsorbed serum albumin. Serum albumin does not as effectively constrict fibronectin's conformation if it is sequentially, rather than simultaneously, introduced, suggesting that serum albumin's crowding mechanism is dependent on its ability to sterically block fibronectin's unfolding during the process of adsorption. Because fibronectin's conformation is dependent on interfacial macromolecular crowding under in vitro conditions, it is important to consider the role of in vivo crowding on protein activity.



ontrolling interfacial protein conformation is important ✓ for the rational design of safe and effective medical biomaterials.^{1,2} Proteins adsorbed to medical nanoparticles (NPs) can interfere with cellular processes^{3,4} or induce NP aggregation⁵⁻⁷ because adsorption and conformation are sensitive to local chemical and physical properties⁸⁻¹³ as well as concentration and composition. 14 Mobile biomaterials may experience changes in local environment that can affect previously adsorbed proteins.¹⁵ Crowding in particular can affect protein conformation, 16-21 yet many surface-adsorbed protein studies do not consider crowding conditions. 13,22 Even in single-component protein experiments, crowding influences protein conformation as a function of concentration. 12,23,24 For example, at physiologically relevant BSA concentrations, BSA forms a stable monolayer on NPs with no detectable conformational changes, 25-27 but at low BSA concentrations, BSA was reported to unfold and induce NP aggregation.5 Because BSA is the most abundant protein in blood and is the dominant adsorbed species when surfaces are exposed to serum, ²⁸⁻³⁰ BSA might serve as a crowding agent at interfaces.

Numerous studies explored serum protein conformation on albumin-crowded surfaces, but questions about mechanistic details between different proteins remain. Fibronectin (Fn) is an abundant and large serum protein that exhibits compact quaternary structure in solution and can unfold to contour lengths >100 nm at interfaces. Fn participates in cellular adhesion and wound healing then its conformational changes expose arginine-glycine-aspartate (RGD) epitopes that interact with cells integrin receptors. Fn's conformational stability is influenced by self-crowding, the interactions with the more abundant human serum albumin (HSA) are

likely crucial.³⁰ Several prior studies of interfacial Fn conformation did not consider HSA crowding or, if they did, used higher Fn/HSA ratios than are physiologically relevant.^{38,39} Fn/HSA layers were compared to self-crowded Fnonly layers^{30,38–43} but without considering HSA's direct influence on dispersed Fn. Conventional ensemble-averaged methods (e.g., quartz crystal microbalance, ^{38,40,44} circular dichroism, ^{16,42} Fourier-transform infrared spectroscopy ^{37,45,46}) can lack the sensitivity to study Fn conformation in HSA-dominated conditions. 40 How different proteins compete for surface space to adsorb and unfold is therefore not entirely understood. For instance, several groups reported that HSA displaced substrate-bound Fn at the ensemble level. 44,47 Because proteins generally experience conformational changes when they initially interact with a substrate,2 displacement would suggest that HSA can modify Fn's conformation. However, other work proposed that preadsorbed Fn,³⁸ and other proteins, 48 resisted displacement. New experimental methods are necessary to answer mechanistic questions about how HSA crowds Fn in competitive scenarios.

In contrast to these ensemble studies, single-molecule fluorescence imaging strategies can sensitively probe a single surface-adsorbed protein's conformation under physiologically relevant conditions and can provide new insights on mechanistic details. Förster resonance energy transfer

Received: November 21, 2019 Accepted: January 22, 2020 Published: January 22, 2020



(FRET) spectroscopy can measure the distance between donor and acceptor fluorophores attached to specific protein residues as a function of the fluorophores' relative intensity with ~ 1 nm resolution. ^{49–52} However, FRET is limited to distances less than 10 nm. ^{13,49,53,54} Single-molecule high resolution imaging with photobleaching (SHRImP)⁵⁵ is one of several techniques that can "superlocalize" single emitters below the diffraction limit of light ^{57–60} and measure the distance between two emitters on the same biomolecule with <20 nm resolution. ^{61,62} Superlocalization techniques are applicable for studying larger ranges of protein conformation, such as those explored by cadherin ⁶³ and Fn, ²² and can track single proteins in complex environments like the actin cytoskeleton ⁶⁴ and extracellular matrix. ^{65,66}

In the current work, we applied SHRImP to determine the mechanism by which HSA crowds surface-adsorbed Fn on aminosilanized glass. After generating interdye distance distributions for Fn in varying crowding conditions, we assessed the influence crowding has on Fn conformation. First, we tested whether the concentration of HSA influences its crowding effect on Fn when both proteins are exposed to the substrate simultaneously. HSA-containing conditions are physiologically relevant while the Fn-only condition represents a common experimental simplification. Next, we varied protein exposure order to test whether HSA's crowding mechanism relies on HSA sterically blocking space prior to Fn unfolding or HSA's interference with Fn-substrate attraction. These protein environment changes are physiologically relevant for mobile biomaterials, like NPs, that experience dynamic environments.

Single-Molecule Measurements. Single Alexa 546-labeled Fn (Fn-546) unfolding was imaged with sub-diffraction-limited precision using SHRImP (Figure 1). We labeled dimeric Fn's four free cysteine residues of known location (Figure S1A) with Alexa 546 maleimide.⁶⁷ We then exposed Fn-546 with and without HSA to an aminosilanized glass surface (Figure 1A) and imaged the surface-adsorbed Fn-546's emission with a widefield total internal reflection fluorescence (TIRF) configuration (Figure 1B). We chose an amine-terminated substrate because it is an appealing biomaterial surface chemistry due to its hydrophilicity and tendency to decrease nonspecific protein adsorption.⁶⁸ SHRImP was performed as follows: After identifying single Fn-546 in an image (Figure 1C), we monitored the intensity of each single Fn-546 over time to identify photobleaching steps using a step transition and state identification (STaSI) algorithm (Figure 1D).⁶⁹ As shown in Figure 1D, individual Alexa 546 emitters were isolated via image subtraction: two-emitter image minus oneemitter image. Resulting emission profiles were superlocalized via 2D Gaussian fitting, allowing interdye distances to be calculated. To determine the localization precision of our SHRImP method, we measured Alexa 546-dual-labeled duplex DNA rulers of known length (Figure S2). We calculated that our SHRImP method has an 8 nm experimental localization precision. Supporting Information section 2a contains additional details about the DNA controls and localization calculations.

Influence of HSA Concentration on Fn Unfolding. Fn-546 unfolds less in the presence of HSA. We exposed Fn-546 to aminosilanized glass with varying concentrations of HSA (0–45 mg/mL) and performed SHRImP analysis on photobleaching movies. Each experiment was performed in triplicate, and individual trials are depicted as complementary cumulative distribution functions (CCDFs) in Figure S3. Figure 2 shows

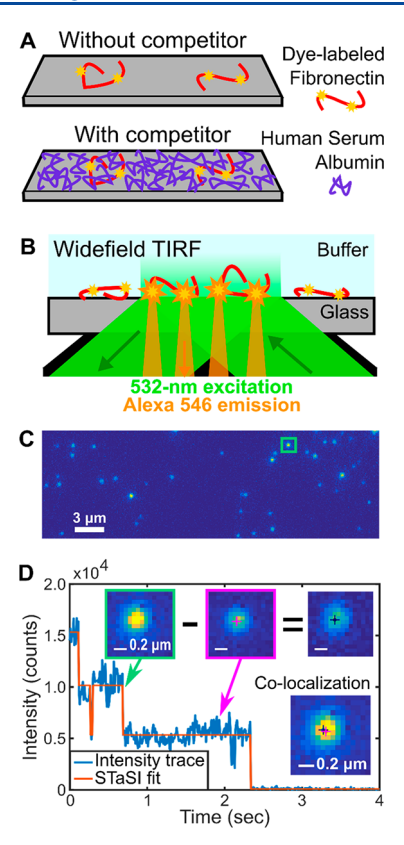


Figure 1. Super-resolved Fn-546 unfolding quantified with SHRImP. (A) Sample preparation: Fn-546 adsorbs to an aminosilanized glass surface with or without unlabeled HSA. (B) Excitation scheme: Widefield objective-based TIRF microscopy collects Fn-546's emission. (C) Example widefield image of surface-adsorbed Fn-546. (D) SHRImP⁵⁵ applied to single Fn-546 in the green box in panel C showing photobleaching steps identified with the STaSI algorithm. The inset shows the image subtraction used to isolate single emitters that bleach during each step. Superlocalization is performed on the single-emitter images (pink and subtracted).

the combined data. We represent the distance distribution of each experimental condition as an averaged histogram from multiple trials. The histograms reveal that surface-adsorbed Fn-546 unfolding produced skewed distributions. The range of interdye distances is consistent with Fn-546's size and the dye locations. In solution, Fn-546's labels are <16 nm apart due to its native globular quaternary conformation. On surfaces, Fn rearranges and produces an elongated rod-like structure with possible distances of 86 nm or larger. The observed range of distances is similar to the Vogel group's earlier measurements of uncrowded Fn adsorbed to hydrophilic surfaces using a similar method.

We observed that the uncrowded Fn-only interdye distance distribution exhibits a greater prevalence of large distances compared to HSA-crowded conditions. Figure 2B compares CCDFs on a logarithmic *y*-axis to accentuate the distributions' tails. Shaded regions indicate the standard deviation of triplicate trials that were averaged. Here, the Fn-only distribution diverges from the HSA-crowded distributions. The inset in Figure 2B shows how the fraction of interdye distances larger than 50 nm varies as a function of HSA concentration. On the basis of error bars in both the CCDFs (Figure 2B) and the fraction of larger than 50 nm distances (inset of Figure 2B), we can distinguish Fn-only from all HSA-crowded conditions, but not the HSA-crowded conditions

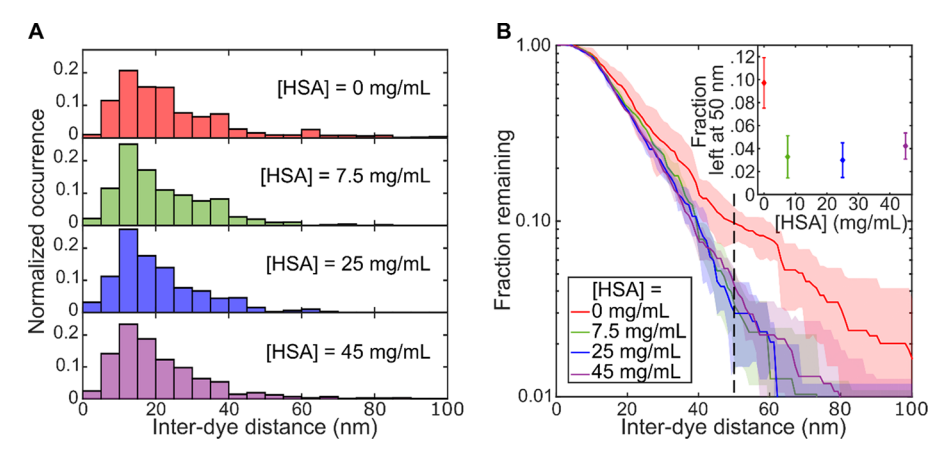


Figure 2. Fn-546's interfacial unfolding is restricted by HSA crowding. (A) Distributions of SHRImP-determined interdye distances on single surface-adsorbed Fn-546 with varying concentration of HSA shown as averaged 5 nm binned histograms from triplicate experiments. (B) CCDFs of the same distributions. The dashed line indicates 50 nm, corresponding with the inset that depicts the fraction of the distribution that exhibits interdye distances larger than 50 nm. Shaded regions and error bars represent the standard deviation among triplicate experiments for each condition.

from each other. As further proof of the quantitatively distinct unfolding distributions observed for Fn-only versus HSA-crowded conditions, the Kolmogorov–Smirnov (K–S) statistical test for non-normal data reveals that the Fn-only statistically differs from all HSA-crowded conditions with 95% confidence (p < 0.05, Table S1).

Our results suggest that HSA crowding prevents Fn-546 from accessing open conformations that are possible in uncrowded conditions. Previous single-molecule measurements showed that surface-adsorbed Fn exhibits many possible conformations. 22,33,70 Uncrowded Fn-546 exhibits a higher occurrence of >50 nm interdye distances than HSA-crowded Fn-546 (Figure 2), indicating that Fn-546 explores additional unfolded conformations in the absence of HSA. Earlier insolution studies of various proteins found that macromolecular crowding limits the number of states a protein can access via the excluded volume effect, in which short-range repulsive interactions between crowding agents favor compact configurations. 18,19 At interfaces, steric repulsion between neighboring adsorbed proteins also influences conformation. Ensemble Fourier-transform infrared spectroscopy measurements of Fn adsorbing to surfaces over time revealed that collective surfaceadsorbed Fn exhibited decreasing levels of denaturation as more Fn bound to the surface,³⁷ suggesting that Fn sterically crowds itself. Our results indicate that HSA crowding sterically limits Fn-546's unfolding. We hypothesize two possible mechanisms for HSA crowding: (1) HSA occupies surface sites before adsorbed Fn can unfold, or (2) HSA displaces Fn or forces its refolding even after Fn has adsorbed and unfolded. In our first set of experiments, HSA reaches the surface faster than Fn-546 due to its higher abundance,⁷¹ and as a result, HSA outcompetes Fn at physiologically relevant ratios.³ However, prior work also illustrated that HSA displaces Fn on a variety of surface types, suggesting that HSA modifies the Fnsubstrate interaction even after Fn has adsorbed and unfolded.44,47

Our assessment of Fn-546's conformation provides mechanistic support for earlier studies, but functional outcomes of Fn's crowding depend on many factors. Fn's functionality relies on availability of its RGD epitopes, located in each monomer's FnIII-10 module, that interact with cells' integrin receptors. ³⁶ Fn-546's cysteine labels are located on either side of the RGD

region (FnIII-7 and FnIII-12).67 Therefore, differences in SHRImP distances describe conformational changes that could affect integrin's accessibility. Zelzer and co-workers found that Fn coadsorbed with HSA on hydrophilic amino plasma polymers at physiological concentration ratios exhibited stronger cellular adhesion than Fn adsorbed alone.⁴³ On the basis of quartz crystal microbalance dissipation experiments, they proposed that HSA crowding inhibits Fn unfolding.⁴³ Our quantification of Fn-546's conformation with and without HSA crowding confirms that HSA restricts Fn unfolding. However, increased crowding does not always improve Fn's activity. It has been reported that lower, rather than higher, densities of surface-bound Fn improves cellular attachment 24,72,73 due to greater RGD region exposure. 72,73 Similarly, Fn adsorbed to hydrophilic gold surfaces exhibited decreased RGD exposure when coadsorbed with HSA,³⁹ possibly suggesting that HSA crowds Fn too much on that surface. In contrast, HSA's presence improved Fn's RGD exposure on hydrophobic surfaces.³⁸ Because Fn exhibits decreased cellular adhesion capabilities⁷³ and increased unfolding²² on hydrophobic surfaces, crowding is expected to help Fn resist denaturation. Although Fn's functionality depends on surface chemistry and other factors, our findings provide support for the mechanism that crowding stabilizes Fn conformation.

Influence of Protein Exposure Order on Fn Unfolding. Fn-546 unfolding is sensitive to the order of exposure to crowding by HSA. In order to assess the impact of exposure order on Fn conformation, we allowed Fn-546 to interact with aminosilanized glass for 30 min prior to introducing 45 mg/mL HSA. The resulting SHRImP-determined distance distribution is similar to the Fn-only condition in that there is an extended distribution of large interdye distances (Figure 3A, Figure S4). Figure 3A shows the pre-exposed Fn-546 condition (Fn-then-HSA) as a CCDF alongside the previously discussed conditions: Fn-only and Fn-546 plus 45 mg/mL HSA (Fn + HSA). Using the K—S comparison, we find that Fn-then-HSA is statistically similar to Fn-only but distinguishable from Fn + HSA (Table S1).

Our results show that HSA's ability to restrict Fn-546's unfolding depends on exposure order. Not only does changing exposure order allow us to explore HSA's crowding mechanism, but it also has physiological relevance for mobile

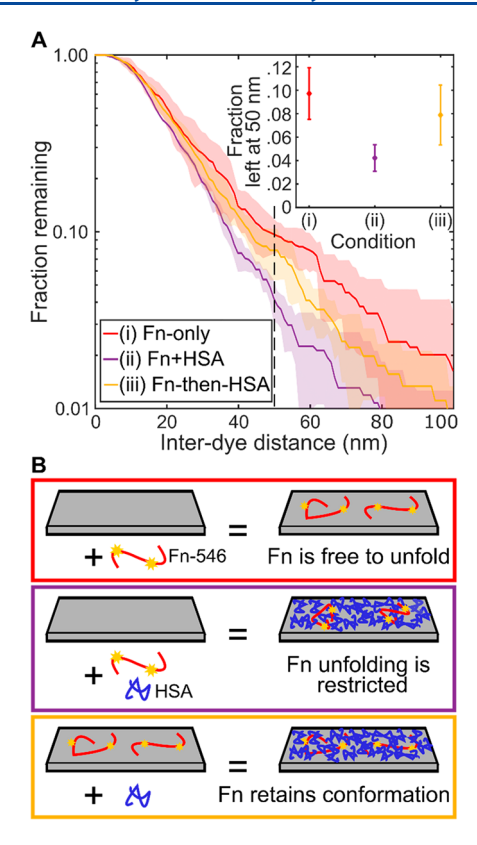


Figure 3. Sequentially introduced HSA is less effective at restricting Fn-546's unfolding than simultaneously exposed HSA. (A) CCDFs of SHRImP-determined interdye distances on single surface-adsorbed Fn-546 under conditions with no HSA (Fn-only, red), coadsorption with HSA (Fn + HSA, purple), and sequential exposure to HSA (Fn-then-HSA, yellow). The dashed line indicates 50 nm, corresponding with the inset that depicts the fraction of the distribution that exhibits interdye distances larger than 50 nm. Shaded regions and error bars represent the standard deviation among triplicate experiments for each condition. (B) Illustrations of Fn-546 conformation in the conditions described in panel A with color-coded boxes.

biomaterials that experience changing protein environments in the body. 15 We propose two mechanisms: (1) HSA prevents Fn unfolding by occupying substrate space before Fn unfolds, and (2) HSA displaces Fn or forces its refolding after Fn already adsorbed. If mechanism 1 is true then the Fn-then-HSA SHRImP distribution would be similar to the Fn-only distribution, and if mechanism 2 is true then the Fn-then-HSA distribution would be similar to the Fn + HSA distribution. Because K-S statistics distinguish the Fn-then-HSA and Fn + HSA distributions, but not Fn-then-HSA and Fn-only (Table S1), we conclude that mechanism 1 plays the most significant role in HSA crowding. We propose the adsorption model depicted in Figure 3B: When Fn-546 adsorbs to a surface without crowding, it achieves its most unfolded configuration possible on that surface type. When Fn-546 coadsorbs with HSA, HSA restricts Fn-546's unfolding. In contrast, if Fn-546 interacts with the surface before HSA's sequential introduction, Fn-546 maintains a fraction of its unfolded configuration. However, the Fn-then-HSA distance distribution in Figure 3A exhibits decreased unfolding compared to Fn-only, which could suggest that HSA also partially alters Fn-546's conformation via mechanism 2. Other studies have reported varying results, including unchanged Fn conformation when denaturant was introduced, 22 and dependence on order of adsorption. 12,37,43,74 Although HSA displaces Fn in certain conditions, HSA does not as effectively displace Fn that is preadsorbed at low surface densities. 47 Overall, the data supports the importance of both the surface chemistry and the available surface area for additional protein adsorption, and our described mechanism is consistent with these earlier results.

In summary, we identified the mechanism by which HSA restricts Fn-546's surface-induced unfolding. By using SHRImP to measure interdye distances on single Fn-546, we quantified Fn-546's unfolding in an HSA-dominant environment. First, we found that uncrowded Fn-546 exhibits a higher fraction of large interdve distances than Fn-546 crowded with varying amounts of HSA. Our finding that HSA crowding modifies Fn's conformation emphasizes the importance of considering physiologically relevant crowding conditions when simulating realistic protein-biomaterial interactions. Second, we varied order of protein exposure to determine the mechanism by which HSA restricts Fn-546 conformation. We observed that Fn-546's conformation was not as significantly restricted when the HSA was introduced sequentially rather than simultaneously. Our results suggest that HSA's crowding mechanism is dominated by HSA blocking surface space before Fn-546 adsorbs and unfolds. Our results provide useful insight into the conformation behavior that preadsorbed proteins on mobile biomaterials may experience in the body's dynamic protein environments. Such restricted conformations could influence the protein's physiological activity, and relevant future work includes studying how the crowding effect influences Fn's cellular adhesion activity. We further stress that techniques such as single-molecule fluorescence imaging are well-suited for studying protein conformation in appropriate conditions.

■ EXPERIMENTAL METHODS

Chemicals and Materials. Phosphate buffered saline (PBS, 20 mM phosphate, 150 mM NaCl) was prepared from 0.1 M phosphate solution and 5 M NaCl solution acquired from Sigma-Aldrich. Human Fn (Chemicon, FC010) and HSA (fraction V, 12668) were obtained from Sigma-Aldrich. Alexa 546 C_5 maleimide (Invitrogen, A10258) was obtained from ThermoFischer. Molecular Biology grade Water and PD-10 desalting columns were obtained from GE Healthcare. Custom Alexa 546-labeled duplex DNA rulers were ordered from Integrated DNA Technologies. Glass coverslips (22 \times 22 mm²) were obtained from VWR. Vectabond reagent ((3-aminopropyl)triethylsilane) was obtained from Vector Laboratories (Burlingame, CA). Custom silicone templates (43018M) were obtained from GraceBioLabs. Other solvents, such as acetone and methanol, were obtained from Sigma-Aldrich.

Fn Conjugation and Characterization. We conjugated Fn with Alexa 546 C_5 maleimide to produce Fn-546 using an adapted protocol (details in Supporting Information section 1a). Fn is composed of three types of repeated domains (I, II, and III) that altogether produce a ~140 nm contour length. 34,36,54,75,76 Alexa 546 maleimide targets four possible free cysteine residues on FnIII-7 and FnIII-15 modules (Figure S1A). Absorbance measurements confirmed a 3–4 dyes/Fn labeling density (Figure S1B). Circular dichroism spectroscopy (J-815 JASCO CD spectrometer) validated Fn's retained tertiary and secondary structure before and after conjugation (Figure S1C).

Sample Preparation. Glass coverslips were cleaned and aminosilanized (Supporting Information section 1b). Sample wells were produced using custom silicone templates. The

concentration of Fn-546 solutions used varied for each experimental condition tested and was optimized to achieve an imaging density of ~ 10 Fn-546/100 μ m² (Supporting Information section 1b). A 40 µL protein solution, containing Fn-546 (2.5–100 pM) with or without HSA (7.5–45 mg/mL) in PBS, was placed in the sample chamber and left to incubate in a dark and humid environment for 30 min. Unbound protein was removed with five washes of 40 μ L of PBS; first the 40 μ L of PBS was gently dropped onto the protein sample, and then 40 µL was removed slowly via pipet so as to not dehydrate or disturb the adsorbed proteins. For experiments with Fn-then-HSA sequential exposure, a 45 mg/mL HSA solution was introduced by the same method of PBS washing. A PBS wash followed the second incubation. A plasma-cleaned glass coverslip was placed over the silicone template to protect the sample. DNA samples were prepared similarly and adsorbed to aminosilanized glass from a 15 pM solution.

Single-Molecule Measurements. Measurements were performed on a home-built TIRF widefield microscope. Excitation light from a 532 nm diode-pumped solid-state laser (Coherent, Compass 315M-100SL, 10 mW before reaching the objective) was focused on the back edge of a high numerical aperture oilimmersion objective (100×, NA = 1.46, Alpha Plan-APO, Carl Zeiss) to achieve total internal reflection. Fluorescence was collected through the same objective and passed through a 2.5× lens, a dichroic mirror (Chroma z532/rpc633), and 532 nm notch filter (Kaiser, HNPF-532.0-1.0). The light then entered a Cairn Optosplit II and passed through a band-pass filter (Chroma, 585/65) before entering the EMCCD camera (Andor, iXon 897). Fn-546 data were collected with 10 ms integration time and 300× electron multiplying gain. For each $10 \times 30 \ \mu m$ region, a 1000-frame video was collected, monitoring the fluorescence and photobleaching of surfaceadsorbed Fn-546. Photobleaching before data acquisition was minimized and positional error due to stage drift was determined to be negligible (Supporting Information section

Single-Molecule Data Analysis. Video files were processed with lab written Matlab code. Emitters were identified from a signal-to-noise-ratio boosted image of the first frame and a trajectory file was created following those identified emitters' positions over each frame of the video. Intensity time traces were generated by summing the central 3×3 pixel intensities for each emitter in each frame, and a STaSI algorithm⁶⁹ was used to identify photobleaching steps. Traces with 2-4 photobleaching steps were deemed eligible for further analysis. Two images for SHRImP subtraction were generated by summing frames in each state (before and after the second-tolast photobleaching event). When the postbleach image was subtracted from the prebleach image, an image of the isolated dye—the first to bleach—was achieved, and superlocalization via 2D Gaussian fitting was employed to identify emitter position. Further data processing was performed similarly to Selvin's original implementation of quartet method SHRImP,55 including filtering thresholds for emitter ellipticity and photon counts. More details on DNA ruler control analysis are found in Supporting Information section 2a. Fn-546 interdye distance distributions are shown as averaged histograms and CCDFs, further discussed in Supporting Information section 2b. The error was quantified as the standard deviation among triplicate trials for each experimental condition. Statistical differences were assessed using K-S two-sample comparisons for nonnormal data.

ASSOCIATED CONTENT

Supporting Information

The Supporting Information is available free of charge at https://pubs.acs.org/doi/10.1021/acs.jpclett.9b03446.

Details regarding experimental and computational methods, data analysis, figures of characterization of Fn-546, SHRImP resolution quantification with DNA rulers, trends in triplicate SHRImP experiments, histograms of data in Figure 3, and table of K–S comparison of interdye distances (PDF)

AUTHOR INFORMATION

Corresponding Authors

Christy F. Landes — Department of Chemistry, Smalley Curl Institute, Department of Electrical and Computer Engineering, and Department of Chemical & Biomolecular Engineering, Rice University, Houston, Texas 77005, United States; oorcid.org/0000-0003-4163-6497; Email: cflandes@rice.edu

Stephan Link — Department of Chemistry, Smalley Curl Institute, and Department of Electrical and Computer Engineering, Rice University, Houston, Texas 77005, United States; orcid.org/0000-0002-4781-930X; Email: slink@rice.edu

Authors

Lauren A. Warning — Department of Chemistry, Rice University, Houston, Texas 77005, United States; ⊚ orcid.org/0000-0001-5628-811X

Qingfeng Zhang — Department of Chemistry and Smalley Curl Institute, Rice University, Houston, Texas 77005, United States; Occid.org/0000-0002-7004-9040

Rashad Baiyasi — Department of Electrical and Computer Engineering, Rice University, Houston, Texas 77005, United States

Complete contact information is available at: https://pubs.acs.org/10.1021/acs.jpclett.9b03446

Author Contributions

The manuscript was written through the contributions of all authors. All authors have given approval of the final version of the manuscript.

Notes

The authors declare no competing financial interest.

ACKNOWLEDGMENTS

This work was funded by the Robert A. Welch Foundation (C-1664 to S.L. and C-1787 to C.F.L.) and the National Science Foundation (CHE-1507745 to S.L. and CHE-1808382 to C.F.L.). Q.Z. acknowledges support from the Smalley-Curl Institute at Rice University through a J. Evans Attwell-Welch Postdoctoral Fellowship. We also acknowledge members of the Link and Landes research groups—particularly Sudeshna Chatterjee, Nicholas Moringo, Logan Bishop, Lauren Mc-Carthy, and Jorge Zepeda O—for their insightful discussions. This work was conducted in part using resources of the Shared Equipment Authority at Rice University.

REFERENCES

(1) Ngo, B. K. D.; Grunlan, M. A. Protein Resistant Polymeric Biomaterials. ACS Macro Lett. 2017, 6 (9), 992–1000.

(2) Wei, Q.; Becherer, T.; Angioletti-Überti, S.; Dzubiella, J.; Wischke, C.; Neffe, A. T.; Lendlein, A.; Ballauff, M.; Haag, R. Protein

- Interactions with Polymer Coatings and Biomaterials. *Angew. Chem., Int. Ed.* **2014**, 53 (31), 8004–31.
- (3) Runa, S.; Lakadamyali, M.; Kemp, M. L.; Payne, C. K. TiO2 Nanoparticle-Induced Oxidation of the Plasma-Membrane: Importance of the Protein Corona. *J. Phys. Chem. B* **2017**, *121* (37), 8619–8625.
- (4) Deng, Z. J.; Liang, M.; Monteiro, M.; Toth, I.; Minchin, R. F. Nanoparticle-induced Unfolding of Fibrinogen Promotes Mac-1 Receptor Activation and Inflammation. *Nat. Nanotechnol.* **2011**, *6* (1), 39–44.
- (5) Dominguez-Medina, S.; Kisley, L.; Tauzin, L. J.; Hoggard, A.; Shuang, B.; Indrasekara, A. S.; Chen, S.; Wang, L. Y.; Derry, P. J.; Liopo, A.; Zubarev, E. R.; Landes, C. F.; Link, S. Adsorption and Unfolding of a Single Protein Triggers Nanoparticle Aggregation. ACS Nano 2016, 10 (2), 2103–2112.
- (6) Zhang, Q.; Hernandez, T.; Smith, K. W.; Jebli, S. A. H.; Dai, A. X.; Warning, L.; Baiyasi, R.; McCarthy, L. A.; Guo, H.; Chen, D. H.; Dionne, J. A.; Landes, C. F.; Link, S. Unraveling the Origin of Chirality from Plasmonic Nanoparticle-Protein Complexes. *Science* **2019**, *365* (6460), 1475–1478.
- (7) Wang, H.; Ma, R.; Nienhaus, K.; Nienhaus, G. U. Formation of a Monolayer Protein Corona Around Polystyrene Nanoparticles and Implications for Nanoparticle Aggregation. *Small* **2019**, *15* (22), 1900974.
- (8) Khan, S.; Gupta, A.; Nandi, C. K. Controlling the Fate of Protein Corona by Tuning Surface Properties of Nanoparticles. *J. Phys. Chem. Lett.* **2013**, *4* (21), 3747–3752.
- (9) Garcia, A. J.; Vega, M. D.; Boettiger, D. Modulation of Cell Proliferation and Differentiation through Substrate-dependent Changes in Fibronectin Conformation. *Mol. Biol. Cell* **1999**, *10* (3), 785–798.
- (10) Arima, Y.; Iwata, H. Preferential Adsorption of Cell Adhesive Proteins from Complex Media on Self-assembled Monolayers and Its Effect on Subsequent Cell Adhesion. *Acta Biomater.* **2015**, *26*, 72–81.
- (11) Moringo, N. A.; Shen, H.; Tauzin, L. J.; Wang, W.; Bishop, L. D. C.; Landes, C. F. Variable Lysozyme Transport Dynamics on Oxidatively Functionalized Polystyrene Films. *Langmuir* **2017**, 33 (41), 10818–10828.
- (12) Wertz, C. F.; Santore, M. M. Effect of Surface Hydrophobicity on Adsorption and Relaxation Kinetics of Albumin and Fibrinogen: Single-Species and Competitive Behavior. *Langmuir* **2001**, *17* (10), 3006–3016.
- (13) Faulon Marruecos, D.; Kastantin, M.; Schwartz, D. K.; Kaar, J. L. Dense Poly(ethylene glycol) Brushes Reduce Adsorption and Stabilize the Unfolded Conformation of Fibronectin. *Biomacromolecules* **2016**, *17* (3), 1017–25.
- (14) Kisley, L.; Patil, U.; Dhamane, S.; Kourentzi, K.; Tauzin, L. J.; Willson, R. C.; Landes, C. F. Competitive Multicomponent Anion Exchange Adsorption of Proteins at the Single Molecule Level. *Analyst* **2017**, *142* (17), 3127–3131.
- (15) Lundqvist, M.; Stigler, J.; Cedervall, T.; Berggard, T.; Flanagan, M. B.; Lynch, I.; Elia, G.; Dawson, K. The Evolution of the Protein Corona around Nanoparticles: A Test Study. *ACS Nano* **2011**, *5* (9), 7503–7509.
- (16) Eggers, D. K.; Valentine, J. S. Crowding and Hydration Effects on Protein Conformation: a Study with Sol-gel Encapsulated Proteins. *J. Mol. Biol.* **2001**, 314 (4), 911–922.
- (17) Wang, Z.; Lu, H. P. Single-Molecule Spectroscopy Study of Crowding-Induced Protein Spontaneous Denature and Crowding-Perturbed Unfolding-Folding Conformational Fluctuation Dynamics. *J. Phys. Chem. B* **2018**, 122 (26), 6724–6732.
- (18) Zhou, H. X.; Rivas, G.; Minton, A. P. Macromolecular Crowding and Confinement: Biochemical, Biophysical, and Potential Physiological Consequences. *Annu. Rev. Biophys.* **2008**, *37*, 375–397.
- (19) Giun, D.; Gruebele, M. Weak Chemical Interactions That Drive Protein Evolution: Crowding, Sticking, and Quinary Structure in Folding and Function. *Chem. Rev.* **2019**, *119*, 10691.
- (20) Hilaire, M. R.; Abaskharon, R. M.; Gai, F. Biomolecular Crowding Arising from Small Molecules, Molecular Constraints,

- Surface Packing, and Nano-Confinement. J. Phys. Chem. Lett. 2015, 6 (13), 2546–2553.
- (21) Qin, S.; Zhou, H. X. Effects of Macromolecular Crowding on the Conformational Ensembles of Disordered Proteins. *J. Phys. Chem. Lett.* **2013**, *4* (20), 3429–3434.
- (22) Klotzsch, E.; Schoen, I.; Ries, J.; Renn, A.; Sandoghdar, V.; Vogel, V. Conformational Distribution of Surface-adsorbed Fibronectin Molecules Explored by Single Molecule Localization Microscopy. *Biomater. Sci.* **2014**, 2 (6), 883.
- (23) Stefani, M. Protein Folding and Misfolding on Surfaces. *Int. J. Mol. Sci.* **2008**, 9 (12), 2515–42.
- (24) Matsui, N.; Nozaki, K.; Ishihara, K.; Yamashita, K.; Nagai, A. Concentration-dependent Effects of Fibronectin Adsorbed on Hydroxyapatite Surfaces on Osteoblast Adhesion. *Mater. Sci. Eng., C* **2015**, *48*, 378–83.
- (25) Rocker, C.; Potzl, M.; Zhang, F.; Parak, W. J.; Nienhaus, G. U. A Quantitative Fluorescence Study of Protein Monolayer Formation on Colloidal Nanoparticles. *Nat. Nanotechnol.* **2009**, *4* (9), 577–80.
- (26) Dominguez-Medina, S.; Blankenburg, J.; Olson, J.; Landes, C. F.; Link, S. Adsorption of a Protein Monolayer via Hydrophobic Interactions Prevents Nanoparticle Aggregation under Harsh Environmental Conditions. ACS Sustainable Chem. Eng. 2013, 1 (7), 833–842.
- (27) Dominguez-Medina, S.; McDonough, S.; Swanglap, P.; Landes, C. F.; Link, S. In Situ Measurement of Bovine Serum Albumin Interaction with Gold Nanospheres. *Langmuir* **2012**, *28* (24), 9131–9.
- (28) Tenzer, S.; Docter, D.; Kuharev, J.; Musyanovych, A.; Fetz, V.; Hecht, R.; Schlenk, F.; Fischer, D.; Kiouptsi, K.; Reinhardt, C.; Landfester, K.; Schild, H.; Maskos, M.; Knauer, S. K.; Stauber, R. H. Rapid Formation of Plasma Protein Corona Critically Affects Nanoparticle Pathophysiology. *Nat. Nanotechnol.* **2013**, 8 (10), 772–81.
- (29) Riedel, T.; Riedelova-Reicheltova, Z.; Majek, P.; Rodriguez-Emmenegger, C.; Houska, M.; Dyr, J. E.; Brynda, E. Complete Identification of Proteins Responsible for Human Blood Plasma Fouling on Poly(ethylene glycol)-based Surfaces. *Langmuir* **2013**, 29 (10), 3388–97.
- (30) Grainger, D. W.; Pavon-Djavid, G.; Migonney, V.; Josefowicz, M. Assessment of Fibronectin Conformation Adsorbed to Polytetra-fluoroethylene Surfaces from Serum Protein Mixtures and Correlation to Support of Cell Attachment in Culture. *J. Biomater. Sci., Polym. Ed.* **2003**, *14* (9), 973–988.
- (31) Williams, E. C.; Janmey, P. A.; Ferry, J. D.; Mosher, D. F. Conformational States of Fibronectin. Effects of pH, Ionic Strength, and Collagen Binding. *J. Biol. Chem.* **1982**, 257 (24), 14973–14978.
- (32) Johnson, K. J.; Sage, H.; Briscoe, G.; Erickson, H. P. The Compact Conformation of Fibronectin Is Determined by Intramolecular Ionic Interactions. *J. Biol. Chem.* 1999, 274 (22), 15473–15479
- (33) Bergkvist, M.; Carlsson, J.; Oscarsson, S. Surface-dependent Conformations of Human Plasma Fibronectin Adsorbed to Silica, Mica, and Hydrophobic Surfaces, Studied with Use of Atomic Force Microscopy. *J. Biomed. Mater. Res.* **2003**, *64A* (2), 349–356.
- (34) Engel, J.; Odermatt, E.; Engel, A.; Madri, J. A.; Furthmayr, H.; Rohde, H.; Timpl, R. Shapes, Domain Organizations and Flexibility of Laminin and Fibronectin, Two Multifunctional Proteins of the Extracellular Matrix. *J. Mol. Biol.* 1981, 150 (1), 97–120.
- (35) Mosher, D. F. Physiology of Fibronectin. *Annu. Rev. Med.* **1984**, 35 (1), 561–575.
- (36) Leahy, D. J.; Aukhil, I.; Erickson, H. P. 2.0 Å Crystal Structure of a Four-Domain Segment of Human Fibronectin Encompassing the RGD Loop and Synergy Region. *Cell* **1996**, *84* (1), 155–164.
- (37) Cheng, S.; Chittur, K. K.; Sukenik, C. N.; Culp, L. A.; Lewandowska, K. The Conformation of Fibronectin on Self-Assembled Monolayers with Different Surface Composition: An FTIR/ATR Study. J. Colloid Interface Sci. 1994, 162 (1), 135–143.

- (38) Giamblanco, N.; Yaseen, M.; Zhavnerko, G.; Lu, J. R.; Marletta, G. Fibronectin Conformation Switch Induced by Coadsorption with Human Serum Albumin. *Langmuir* **2011**, *27* (1), 312–9.
- (39) Giamblanco, N.; Zhavnerko, G.; Tuccitto, N.; Licciardello, A.; Marletta, G. Coadsorption-dependent Orientation of Fibronectin Epitopes at Hydrophilic Gold Surfaces. *Soft Matter* **2012**, *8* (32), 8370.
- (40) Hindie, M.; Camand, E.; Agniel, R.; Carreiras, F.; Pauthe, E.; Van Tassel, P. Effects of Human Fibronectin and Human Serum Albumin Sequential Adsorption on Preosteoblastic Cell Adhesion. *Biointerphases* **2014**, *9* (2), No. 029008.
- (41) Sousa, S. R.; Lamghari, M.; Sampaio, P.; Moradas-Ferreira, P.; Barbosa, M. A. Osteoblast Adhesion and Morphology on TiO2 Depends on the Competitive Preadsorption of Albumin and Fibronectin. J. Biomed. Mater. Res., Part A 2008, 84 (2), 281–290.
- (42) Muzzio, N. E.; Pasquale, M. A.; Rios, X.; Azzaroni, O.; Llop, J.; Moya, S. E. Adsorption and Exchangeability of Fibronectin and Serum Albumin Protein Corona on Annealed Polyelectrolyte Multilayers and Their Consequences on Cell Adhesion. *Adv. Mater. Interfaces* **2019**, *6* (8), 1900008.
- (43) Zelzer, M.; Albutt, D.; Alexander, M. R.; Russell, N. A. The Role of Albumin and Fibronectin in the Adhesion of Fibroblasts to Plasma Polymer Surfaces. *Plasma Processes Polym.* **2012**, 9 (2), 149–156.
- (44) Pegueroles, M.; Tonda-Turo, C.; Planell, J. A.; Gil, F.-J.; Aparicio, C. Adsorption of Fibronectin, Fibrinogen, and Albumin on TiO2: Time-Resolved Kinetics, Structural Changes, and Competition Study. *Biointerphases* **2012**, *7* (1), 48.
- (45) Pandey, L. M.; Pattanayek, S. K.; Delabouglise, D. Properties of Adsorbed Bovine Serum Albumin and Fibrinogen on Self-Assembled Monolayers. *J. Phys. Chem. C* **2013**, *117* (12), 6151–6160.
- (46) Wang, X.; Wang, M.; Lei, R.; Zhu, S. F.; Zhao, Y.; Chen, C. Chiral Surface of Nanoparticles Determines the Orientation of Adsorbed Transferrin and Its Interaction with Receptors. *ACS Nano* **2017**, *11* (5), 4606–4616.
- (47) Renner, L.; Pompe, T.; Salchert, K.; Werner, C. Fibronectin Displacement at Polymer Surfaces. *Langmuir* **2005**, *21* (10), 4571–4577.
- (48) Wertz, C. F.; Santore, M. M. Effect of Surface Hydrophobicity on Adsorption and Relaxation Kinetics of Albumin and Fibrinogen: Single-Species and Competitive Behavior. *Langmuir* **2001**, *17* (10), 3006–3016.
- (49) Selvin, P. R. The Reniassance of Fluorescence Resonance Energy Transfer. *Nat. Struct. Biol.* **2000**, 7 (9), 730.
- (50) Dolino, D. M.; Chatterjee, S.; MacLean, D. M.; Flatebo, C.; Bishop, L. D. C.; Shaikh, S. A.; Landes, C. F.; Jayaraman, V. The Structure-energy Landscape of NMDA Receptor Gating. *Nat. Chem. Biol.* 2017, 13 (12), 1232–1238.
- (51) Manz, C.; Kobitski, A. Y.; Samanta, A.; Keller, B. G.; Jaschke, A.; Nienhaus, G. U. Single-molecule FRET Reveals the Energy Landscape of the Full-length SAM-I Riboswitch. *Nat. Chem. Biol.* **2017**, *13*, 1172–1178.
- (52) Kuzmenkina, E. V.; Heyes, C. D.; Nienhaus, G. U. Singlemolecule Forster Resonance Energy Transfer Study of Protein Dynamics Under Denaturing Conditions. *Proc. Natl. Acad. Sci. U. S. A.* 2005, 102 (43), 15471–15476.
- (53) Rock, R. S.; Rice, S. E.; Wells, A. L.; Purcell, T. J.; Spudich, J. A.; Sweeney, H. L. Myosin VI is a Processive Motor with a Large Step Size. *Proc. Natl. Acad. Sci. U. S. A.* **2001**, *98* (24), 13655–13659.
- (54) Erickson, H. P.; Carrell, N.; McDonagh, J. Fibronectin Molecule Visualized in Electron Microscopy: A Long, Thin, Flexible Strand. *J. Cell Biol.* **1981**, *91* (3), *673*–78.
- (55) Gordon, M. P.; Ha, T.; Selvin, P. R. Single-molecule High-resolution Imaging with Photobleaching. *Proc. Natl. Acad. Sci. U. S. A.* **2004**, *101* (17), 6462–5.
- (56) Shen, H.; Tauzin, L. J.; Baiyasi, R.; Wang, W.; Moringo, N.; Shuang, B.; Landes, C. F. Single Particle Tracking: From Theory to Biophysical Applications. *Chem. Rev.* **2017**, *117* (11), 7331–7376.

- (57) Rust, M. J.; Bates, M.; Zhuang, X. Sub-diffraction-limit Imaging by Stochastic Optical Reconstruction Microscopy (STORM). *Nat. Methods* **2006**, *3* (10), 793–5.
- (58) Betzig, E.; Patterson, G. H.; Sougrat, R.; Lindwasser, O. W.; Olenych, S.; Bonifacino, J. S.; Davidson, M. W.; Lippincott-Schwartz, J.; Hess, H. F. Imaging Intracellular Fluorescent Proteins at Nanometer Resolution. *Science* **2006**, *313*, 1642–1645.
- (59) Backlund, M. P.; Lew, M. D.; Backer, A. S.; Sahl, S. J.; Grover, G.; Agrawal, A.; Piestun, R.; Moerner, W. E. Simultaneous, Accurate Measurement of the 3D Position and Orientation of Single Molecules. *Proc. Natl. Acad. Sci. U. S. A.* **2012**, *109* (47), 19087–92.
- (60) Fu, B.; Isaacoff, B. P.; Biteen, J. S. Super-Resolving the Actual Position of Single Fluorescent Molecules Coupled to a Plasmonic Nanoantenna. *ACS Nano* **2017**, *11* (9), 8978–8987.
- (61) Qu, X.; Wu, D.; Mets, L.; Scherer, N. F. Nanometer-localized Multiple Single-molecule Fluorescence Microscopy. *Proc. Natl. Acad. Sci. U. S. A.* **2004**, *101* (31), 11298–303.
- (62) Churchman, L. S.; Okten, Z.; Rock, R. S.; Dawson, J. F.; Spudich, J. A. Single Molecule High-resolution Colocalization of Cy3 and Cy5 Attached to Macromolecules Measures Intramolecular Distances Through Time. *Proc. Natl. Acad. Sci. U. S. A.* **2005**, *102* (5), 1419–23.
- (63) Pertsinidis, A.; Zhang, Y.; Chu, S. Subnanometre Single-molecule Localization, Registration and Distance Measurements. *Nature* **2010**, *466* (7306), 647–51.
- (64) Biteen, J. S.; Thompson, M. A.; Tselentis, N. K.; Bowman, G. R.; Shapiro, L.; Moerner, W. E. Super-resolution Imaging in Live Caulobacter crescentus Cells using photoswitchable EYFP. *Nat. Methods* **2008**, *5* (11), 947–949.
- (65) Kanchanawong, P.; Shtengel, G.; Pasapera, A. M.; Ramko, E. B.; Davidson, M. W.; Hess, H. F.; Waterman, C. M. Nanoscale Architecture of Integrin-based Cell Adhesions. *Nature* **2010**, *468* (7323), 580–4.
- (66) Fruh, S. M.; Schoen, I.; Ries, J.; Vogel, V. Molecular Architecture of Native Fibronectin Fibrils. *Nat. Commun.* **2015**, *6*, 7275.
- (67) Smith, M. L.; Gourdon, D.; Little, W. C.; Kubow, K. E.; Eguiluz, R. A.; Luna-Morris, S.; Vogel, V. Force-induced Unfolding of Fibronectin in the Extracellular Matrix of Living Cells. *PLoS Biol.* **2007**, 5 (10), e268.
- (68) Bagwe, R. P.; Hilliard, L. R.; Tan, W. Surface Modification of Silica Nanoparticles to Reduce Aggregation and Nonspecific Binding. *Langmuir* **2006**, 22 (9), 4357–4362.
- (69) Shuang, B.; Cooper, D.; Taylor, J. N.; Kisley, L.; Chen, J.; Wang, W.; Li, C. B.; Komatsuzaki, T.; Landes, C. F. Fast Step Transition and State Identification (STaSI) for Discrete Single-Molecule Data Analysis. *J. Phys. Chem. Lett.* **2014**, *5* (18), 3157–3161.
- (70) Erickson, H. P.; Carrell, N. A. Fibronectin in Extended and Compact Conformations. Electron Microscopy and Sedimentation Analysis. *J. Biol. Chem.* **1983**, 258 (23), 14539–14544.
- (71) Vroman, L.; Adams, A. L. Findings with the Recording Ellipsometer Suggesting Rapid Exchange of Specific Plasma Proteins at Liquid/Solid Interfaces. *Surf. Sci.* 1969, 16, 438–446.
- (72) Keselowsky, B. G.; Collard, D. M.; Garcia, A. J. Surface Chemistry Modulates Fibronectin Conformation and Directs Integrin Bidning and Specificty to Control Cell Adhesion. *J. Biomed. Mater. Res., Part A* **2003**, *66A* (2), 247–259.
- (73) Michael, K. E.; Vernekar, V. N.; Keselowsky, B. G.; Meredith, J. C.; Latour, R. A.; Garcia, A. J. Adsorption-Induced Conformational Changes in Fibronectin Due to Interactions with Well-Defined Surface Chemistries. *Langmuir* **2003**, *19* (19), 8033–8040.
- (74) Vilanova, O.; Mittag, J. J.; Kelly, P. M.; Milani, S.; Dawson, K. A.; Radler, J. O.; Franzese, G. Understanding the Kinetics of Protein-Nanoparticle Corona Formation. *ACS Nano* **2016**, *10* (12), 10842–10850
- (75) Baron, M.; Norman, D.; Willis, A.; Campbell, I. D. Structure of the Fibronectin Type I Module. *Nature* **1990**, 345 (6276), 642.

- (76) Price, T. M.; Rudee, M. L.; Pierschbacher, M.; Ruoslahti, E. Structure of Fibronectin and Its Fragments in Electron Microscopy. *Eur. J. Biochem.* **1982**, *129* (2), 359–363.
- (77) Shuang, B.; Chen, J.; Kisley, L.; Landes, C. F. Troika for Single Particle Tracking Programing: SNR Enhancement, Particle Identification, and Mapping. *Phys. Chem. Chem. Phys.* **2014**, *16* (2), 624–634.